ISSN 1001-0742
CN 11-2629/X

2012
Volume 24
Number 4

JOURNAL OF ENVIRONMENTAL SCIENCES

Science Press

Sponsored by
Research Center for Eco-Environmental Sciences
Chinese Academy of Sciences

ISSN 1001–0742 **Journal of Environmental Sciences** Vol. 24 No. 4 2012

CONTENTS

Serial parameter: CN 11-2629/X*1989*m*210*en*P*27*2012-4

Available online at www.sciencedirect.com
ScienceDirect
Journal of Environmental Sciences 2012, 24(4) 750–756
JOURNAL OF ENVIRONMENTAL SCIENCES
ISSN 1001-0742
CN 11-2629/X
www.jesc.ac.cn

Synthesis of TiO_2 nanoparticles in different thermal conditions and modeling its photocatalytic activity with artificial neural network

Fatemeh Ghanbary[1,*], Nasser Modirshahla[2], Morteza Khosravi[1], Mohammad Ali Behnajady[2]

1. Department of Applied Chemistry, Faculty of Chemistry, North Tehran Branch, Islamic Azad University, Tehran, 1913674711, Islamic Republic of Iran. E-mail: F_Ghanbary@iau-tnb.ac.ir; Ghan-bary83@yahoo.com
2. Research Laboratory, Department of Applied Chemistry, Tabriz Branch, Islamic Azad University, Tabriz, 1655, Islamic Republic of Iran

Received 14 April 2011; revised 13 August 2011; accepted 23 September 2011

Abstract

Titanium dioxide (TiO_2) nanoparticles were prepared by sol gel route. The preparation parameters were optimized in the removal of 4-nitrophenol (4-NP). All catalysts were analyzed by X-ray diffraction (XRD) and scanning electron microscopy (SEM). An artificial neural network model (ANN) was developed to predict the photocatalytic removal of 4-NP in the presence of TiO_2 nanoparticles prepared under desired conditions. The comparison between the predicted results by designed ANN model and the experimental data proved that modeling of the removal process of 4-NP using artificial neural network was a precise method to predict the extent of 4-NP removal under different conditions.

Key words: nanoparticle; TiO_2; 4-nitrophenol; photocatalysis; neural network modeling

DOI: 10.1016/S1001-0742(11)60815-2

Introduction

One of the most active areas in environmental research is the development of highly efficient methods for the elimination of hazardous pollutants from air, soil and water (Castro et al., 2008). Recently, chemical treatment methods, based on the generation of hydroxyl radicals, known as advanced oxidation processes (AOPs) have been developed (Behnajady et al., 2007a). AOPs have attracted wide interests in wastewater treatment since the 1990s (Modirshahla et al., 2007).

The development of UV/TiO_2 process to achieve complete mineralization of organic pollutants has been widely tested for a large variety of industrial dyes (Behnajady et al., 2007b). Semiconductors used for such applications should have a high resistance to photocorrosion, water hydrolysis processes and low cost. Their photosensitivity should be efficient when using the solar spectrum and have high quantum efficiency. However, the material having these ideal properties has not been obtained (Bessekhouad et al., 2003). The semiconductor photocatalysis, using titania powders, is recognized as one of the promising techniques for this purpose. In fact, considering photocatalysis research, the synthesis of titania materials with optimized properties has been an actual target of reach (Castro et al., 2008). TiO_2 exists in three different crystalline habits: rutile (tetragonal), anatase (tetragonal) and brookite (orthorombic). All three crystalline structures consist of deformed TiO_6 octahedra connected differently by corners and edges. Rutile is the stable form, whereas anatase and brookite are metastable and can be readily transformed to rutile when heated. Anatase is the phase normally found in the sol gel synthesis of TiO_2 (Di Paola et al., 2008). It is well known that the anatase polymorph presents higher photoactivity when compared to brookite or rutile polymorphs (Castro et al., 2008). Thus, it is important to prepare TiO_2 samples, where parameters such as crystal structure, surface morphology and phase stability, could be controlled and optimized. The effect of various operational parameters on photocatalytic removal of aromatic compounds has been reported (Chwe et al., 2008; Giri et al., 2008; Zhang et al., 2010), but to the best of our knowledge, the application of artificial neural network (ANN) for predicting the performance of 4-NP removal by prepared nano TiO_2, has not been reported.

This work is devoted to the study of the influence of different thermal conditions on the preparation of TiO_2 nanoparticles by sol-gel route. The photocatalytic efficiency of these materials was evaluated in the removal of 4-NP as a refactory.

Because of the complexity of the reactions in a photocatalytic system, a few studies have been conducted involving the kinetics of the photocatalytic removal of organic pollutants. The phenomenological treatment of a photochemical system is, in general, quite complex. This is

* Corresponding author.

caused by the complexity of solving the equations that involve the radiant energy balance, the spatial distribution of the absorbed radiation, mass transfer, and mechanisms of a photochemical photocatalytic removal involving radical species. Due to these reasons, the modeling of the removal process via artificial neural network (ANN) techniques is quite appropriate (Göb et al., 1999; Calza et al., 2008; Pareek et al., 2002; Khataee, 2009).

Therefore another aspect of this work was the development of a multilayer feed-forward neural network model to predict the efficiency of photochemical removal of 4-NP by UV/TiO_2 process.

1 Materials and methods

1.1 Materials

Tetraisopropylorthotitanate $Ti(OC_3H_7)_4$, methanol (MeOH) and 4-NP were obtained from Merck (Germany) and used without any further purifications. Deionized water was used throughout the work.

1.2 Ultrasonic bath (T 460/H)

The ultrasonic bath Elma (GmbH) was used with the operating frequency of 35 kHz and a rated output power of 170 W. The bath has the dimensions of 240 mm×137 mm×100 mm. The total internal body is made from stainless steel.

1.3 Method

To get nanostructured TiO_2, 12 mL $Ti(OC_3H_7)_4$ solution was dissolved in 1.35 mL MeOH and the mixture was sonicated for 3 min and agitated at 70°C for 210 min under magnetic stirrer. Water was added dropwise into the hot solution (70°C) during this period of time. The precipitate was isolated by filtration, washed with hot water and organic solvents to remove the adsorbed impurities, and calcined at different temperatures for 3 hr.

1.4 Photocatalytic experiments

All experiments were carried out in a batch photoreactor. The radiation source was a low pressure mercury UV lamp (30 W, UV-C, λ_{max} = 254 nm, manufactured by Philips, Holland), which was placed above a batch photoreactor of 0.5 L volume. The incident UV light intensity was measured by a Lux-UV-IR meter (Leybold Co. Ltd., Japan). In each experiment, a known amount of TiO_2 was added to 500 mL of the solution and a magnetic stirrer was used in order to achieve a homogeneous mixture.

1.5 Analytical method

In the presence of TiO_2 as photocatalyst, 4-NP was used as pollutant. Sample solutions were sonicated before irradiation for 5 min. At known irradiation time intervals, the samples (5 mL) were taken out and then analyzed by UV-Vis spectrophotometer (Ultrospec 2000, Biotech Pharmacia, England) at 400 nm. A linear correlation was established between the 4-NP concentration and the absorbance, in the range 0–60 mg/L with a correlation coefficient, R^2= 0.9991. The Eq. (1) was used to calculate the photocatalytic removal efficiency (R, %) in the experiments:

$$R = \left(\frac{C_0 - C_t}{C_0}\right) \times 100 \tag{1}$$

where, C_0 (mg/L) and C_t (mg/L) are initial concentration of 4-NP and the concentration of 4-NP at time t.

The crystal structure of the powders was checked by powder X-ray diffraction (XRD) using Siemens X-ray diffraction D5000 with Cu $K\alpha$ radiation. An accelerating voltage of 40 kV and emission current of 30 mA were used. The average crystalline size of the samples was calculated according to the Debye-Scherrer formula (Bartram and Kaelble, 1967; Rodrígerz and Fernández-García, 2007):

$$D = \frac{0.89\lambda}{\beta\cos\theta} \tag{2}$$

where, D (Å) is the average crystallite size, λ is the wavelength of the X-ray radiation (Cu $K\alpha$= 1.54178 Å), β is the full width at half maximum intensity of the peak and θ is the diffraction angle. If a sample contains anatase and rutile forms, the mass fraction of rutile (χ) can be calculated from the following equation (Bessekhouad et al., 2003).

$$\chi = \frac{I_R}{0.8I_A + I_R} \tag{3}$$

where, I_A and I_R represent the integrated intensity of the anatase (101) and rutile (110) peaks, respectively.

Scanning electron microscopy (SEM) of samples was carried out on a Philips XL 30 microscope.

1.6 Artificial neural network software

All ANN calculations were carried out using Matlab 7.8 (2009R) mathematical software with ANN toolbox. A three-layer network with a sigmoidal transfer function with back-propagation algorithm was designed in this study.

2 Results and discussion

2.1 Preliminary results

A thermal treatment is necessary to improve the crystallinity of amorphous compounds. Several syntheses conditions have been assayed. When TiO_2 powders are calcinated at higher temperature, crystal structure transformations may occur. The amorphous-anatase and anatase-rutile transitions depend strongly on the calcination conditions.

The prepared titania nanopowders have been characterized by XRD and SEM (Figs. 1 and 2).

The results for structural and morphological properties of the prepared samples have been presented in Table 1.

Interesting correlations can be established between the morphology and the hydrothermal conditions of preparation. All the prepared samples present heterogeneity in shapes and sizes of nanoparticles. We can ascribe this observation to different crystal growth rates.

Table 1 Crystallization conditions, species of phase and Crystallite size

Sample	Crystallization temperature (°C)	Species of phase		Crystallite size (nm)	
		Anatase (%)	Rutile (%)	Anatase	Rutile
A	400	100	–	6.5	–
B	500	100	–	8	–
C	600	100	–	10.2	–
D	700	78.64	21.36	15.35	26.50
E	800	–	100	–	10.60

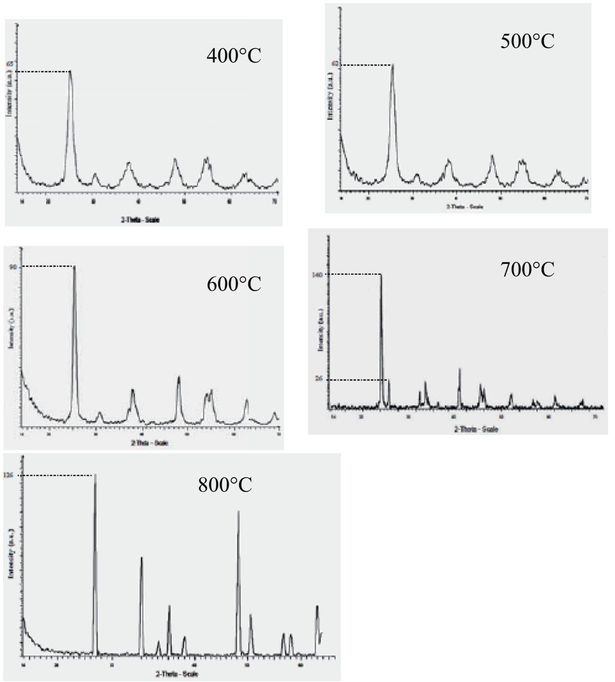

Fig. 1 X-ray diffraction patterns of TiO_2 nanopowders calcinated at 400–800°C.

In order to test and ensure the phase stability of the prepared samples some calcination experiments were performed under different temperatures, ranging from 400 to 800°C. The physical properties of the samples are compared (Table 1), it can be seen that the anatase phase remains pure and stable until 600°C, some rutile conversion starting at 700°C and the change of anatase to rutile phase was completed at 800°C where the grain sizes of samples are different. This is due to the fact that at low temperatures, the crystallization is slow, and it performs at low rate and a more homogeneous way (Castro et al., 2008).

2.2 Photocatalytic studies

To examine the photocatalytic activity of the prepared samples, the photocatalytical removal of 4-NP in presence of nonopowders was studied. The results have been given in Fig. 3. It is found that the photocatalytic performance of various TiO_2 samples decreased in the following order of: 400 > 500 > 600 > 700 > 800°C.

The results can be explained in terms of the preparation steps involved in the synthesis of these samples. Photocatalytic activity of mesoporous TiO_2 is strongly dependent on its phase structure, crystallite size and pore structure (When et al., 2005). It is well known that anatase type TiO_2 has higher photocatalytic activity than rutile type TiO_2 and in anatase phase, the samples with small grain size have higher photocatalytic activity than the others, which also is consistent with the experimental results (Ambrus et al., 2008; Yang et al., 2005). Additionally, it

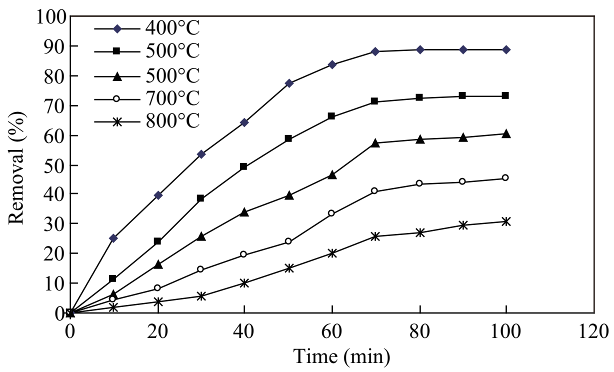

Fig. 3 Removal percentage of 4-NP in the presence of TiO_2 nanophotocatalysts (refer to Figs. 1 and 2). Conditions: nano TiO_2 concentration 0.04 g/L, initial 4-NP concentration 20 mg/L, UV 30.3 W/m^2.

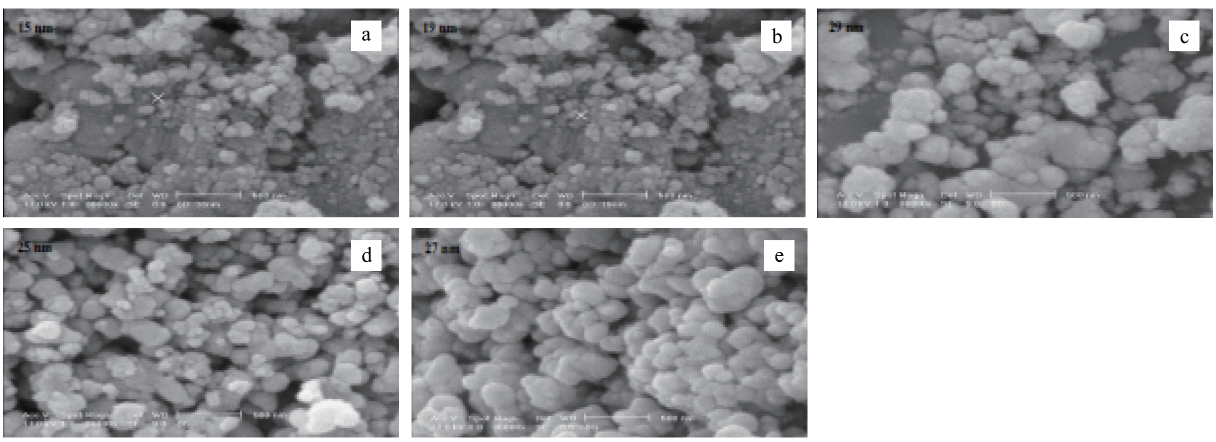

Fig. 2 SEM images of TiO_2 nanopowders calcinated at 400–800°C. (a) 400°C; (b) 500°C; (c) 600°C; (d) 700°C, (e) 800°C.

has been reported that calcination also reduces the number of hydroxyl ions on the surface of the catalyst, leading to an overall reduction in the photoactivity of catalysts (Yang et al., 2005). The effect of operational parameters such as irradiation time, UV light intensity and 4-NP initial concentration with various amount of nano TiO_2 (sample A) was studied.

2.3 Neural network modeling

ANNs are direct inspiration from the biology of human brain, where billions of neurons are interconnected to process a variety of complex information. Accordingly, a computational neural network consists of simple processing units called neurons (Gontarski et al., 2000; Slokar et al., 1999). In general, a neural net (multilayered perceptron), as shown in Fig. 4, has interconnected structure in parallel form consisting of: (1) input layer of neuron (independent variables), (2) a number of hidden layers, (3) output layer (dependent variables). The number of input and output neurons is fixed by the nature of the problem. The hidden layers act like feature detectors can be more than one hidden layer. Universal approximation theory, however, suggests that a network with a single hidden layer with a sufficiently large number of neurons can interpret any input-output structure (Daneshvar et al., 2006).

The topology of an ANN is determined by the number of layers in the ANN, the number of nodes in each layer and the nature of the transfer functions. Correct identification of the set of independent input variables and the output variables is the first task in building ANN model for a process. Optimization of ANN topology is probably the next important step in the development of a model. We used threelayered feed forward back propagation neural network (4:14:1) for modeling of UV/TiO_2 process (Fig. 4). In the present work, the input variables to the feed forward neural network were as follows: initial nano TiO_2 dosage (mg/L), removal time (min), UV light intensity (W/m^2), initial concentration of 4-NP (mg/L). 4-NP removal percentage (R, %) was chosen as the experimental response or output variable.

In this work, we tested different numbers of neurons, from 2 to 20, in the hidden layer. Each topology was repeated three times to avoid random correlation due to the random initialization of the weights. Figure 5 illustrates the relation between the network error and the number

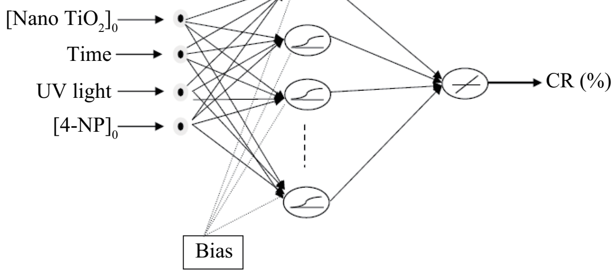

Fig. 4 Structure of the used ANN in the present study.

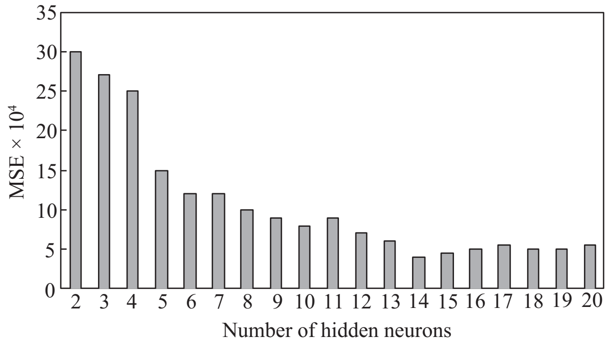

Fig. 5 Effect of the number of neurons in the hidden layer on the performance of the neural network. MSE: mean square error.

of neurons in the hidden layer. The mean square error (MSE) was used as the error function. MSE measures the performance of the network according to the following equation:

$$\mathrm{MSE} = 1/N \sum_{i=1}^{N} (t_i - a_i)^2 \tag{4}$$

where, N is the number of data point, t_i the network prediction, a_i experimental response and i is an index of data. We can see that the performance of the network stabilized after inclusion of an adequate number of hidden units just about fourteen. The network with few neurons in the hidden layer cannot converge effectively.

In this work, for threelayer network the sigmoid (log(sig)) and linear (Purel(in)) transfer functions were used as transfer functions in hidden and output layers, respectively. The train gradient descent with momentum and adaptive learning rate (traingdx), as a transfer function and the training-and-test method were used to evaluate the ANN. Traingdx is a network training function that updates weight and bias values according to gradient descent and an adaptive learning rate. The range of variables studied is summarized in Table 2. Totally 147 experimental sets were used to feed the ANN structure. The data sets were divided into training, validation and test subsets, each of which contains 75, 36 and 36 samples, respectively. The validation and test sets, for the evaluation of the validation and modeling power of the networks, were randomly selected from the experimental data.

For the best result all samples from the training, validation and test sets were scaled to a new value with *premnx* function in Matlab. In order to calculate training, validation and test error, all of the predicted responses by *postmnmx* function in Matlab (outputs) were returned to their original scale and compared them with experimental responses.

Table 2 Range of studied variables

Variable	Range
Input layer	
Nano TiO_2 initial dosage (g/L)	0.01–0.05
Time (min)	0–60
UV light intensity (W/m^2)	8.6–45.3
4-NP initial concentration (mg/L)	5–50
Output layer	
Removal of 4-NP (%)	0–100

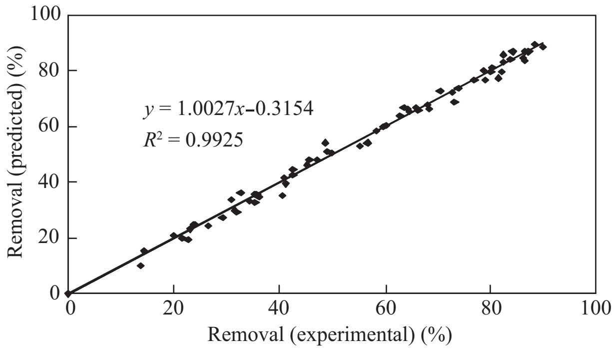

Fig. 6 Comparison of the experimental results with values calculated via neural network modeling for test set.

Training initial weights were randomly selected and training was terminated when the error gradient was less than 10^{-3}. A weakness of the neural network is that it can be easily overfitted, causing the error rate on validation data to be much larger than the error rate on the training data. It is therefore important not to overtrain data. Overfitting is more likely to occur at later epochs than earlier ones. A good method for choosing the number of training epoch is to use the validation data set periodically to compute the error rate for it while the network is being trained. The validation error decreases in the early epochs of backpropagation but after a while, it begins to increase. The point of minimum validation error is a good indicator of the best number of epochs for training and the weight at that stage are likely to provide the best error rate in new data (Khataee and Mirzajani, 2010; Khataee et al., 2011). Our results indicated that the minimum error of the validation set could be achieved in the epochs just about 4000.

Figure 6 shows a comparison between calculated and experimental values of the output variable for test sets by using neural network model. Plot in this figure has correlation coefficient of 0.9925 for test set. These results confirmed that neural network model reproduces the removal in this system, within experimental ranges adopted in the fitting model.

The neural net weight matrix can be used to assess the relative importance of the various input variables on the output variables. It was proposed an equation based on the partitioning of connection weights (Aleboyeh et al., 2008):

$$I_j = \frac{\sum_{m=1}^{m=N_\mathrm{h}} \left(\left(\left| W_{jm}^{\mathrm{ih}} \right| \Big/ \sum_{k=1}^{N_i} \left| \mathrm{W}_{km}^{\mathrm{ih}} \right| \right) \times \left| W_{mn}^{\mathrm{ho}} \right| \right)}{\sum_{k=1}^{k=N_\mathrm{i}} \left\{ \sum_{m=1}^{m=N_\mathrm{h}} \left(\left| W_{km}^{\mathrm{ih}} \right| \Big/ \sum_{k=1}^{\mathrm{N}_i} \left| \mathrm{W}_{km}^{\mathrm{ih}} \right| \right) \times W_{mn}^{\mathrm{ho}} \right\}} \quad (5)$$

where, I_j is the relative importance of the jth input variable on the output variable, N_i and N_h are the numbers of input and hidden neurons, respectively, Ws are connection weights, the superscripts 'i', 'h' and 'o' refer to input, hidden and output layers, respectively, and subscripts 'k', 'm' and 'n' refer to input, hidden and output neurons, respectively.

The relative importance of input variables on the value of 4-NP removal efficiency was calculated by Eq. (4) and shown in Table 3. As can be seen, all of the variables have strong effects on the 4-NP removal efficiency. But the effect of 4-NP initial concentration is more than others. Therefore, none of the variables studied in this work could have been neglected in the present analysis.

Table 3 Relative importance of input variables on the value of 4-NP removal efficiency

Input variable	Importance (%)
Nano TiO_2 (g/L)	23.9
Time (min)	26.1
UV light intensity (W/m^2)	19.9
4-NP initial concentration (mg/L)	30.1

2.4 Parameters on photodegradation efficiency

Figure 7 shows the photocatalytic removal of 4-NP in aqueous solution under different conditions.

2.4.1 Nano TiO_2 dosage

The photocatalytic removal of 4-NP in aqueous solution with various nano TiO_2 dosage (prepared at 400°C was studied. The experimental and ANN calculated values of removal are shown in Fig. 7a. Apparently, the photodegradation efficiency of 4-NP increased when the concentration of TiO_2 increased from 0.01 to 0.05 g/L. After 60 min of irradiation, about 88.26% of 4-NP degraded in the aqueous solution with 0.04 g/L TiO_2, while only 26% of 4-NP was photodegraded at 0.01 g/L TiO_2 suspended solution. This was mainly because of the increase of hydroxyl radical produced from irradiated TiO_2. The optimum amount of TiO_2 should be added to avoid superfluous catalyst and also to ensure total absorption of radiation photons for efficient photodegradation (Habibi et al., 2005; Muruganandham and Swaminathan, 2006; Zhang et al., 2008). When we increased the dose of the catalyst, of course, it would increase the adsorption amount of the reaction target resulting in a faster degradation rate. However, high dosage of TiO_2 particles became much easier to aggregate and reduced the light transmission. The comparison between ANN and experimental data in Fig. 7 shows that the results are in good agreement.

2.4.2 Irradiation time

Reaction time influences the treatment efficiency of the UV/TiO_2 process. Figure 7b shows the relationship between the removal efficiency and the photocatalytic reaction time. According to the results shown in Fig. 7b the optimum reaction time was 60 min for 4-NP removal from solution. It shows good agreement between predictions from ANN model and experimental results. From this plot it can be seen that obtained results from the proposed ANN model are in good agreement with the experimental data.

2.4.3 UV light intensity

The variation between experimental and ANN calculated values of 4-NP removal efficiency during the reaction period under different UV light intensity have been presented in Fig. 7c. The figure clearly shows that the removal rate increases by increasing UV irradiation intensity. The

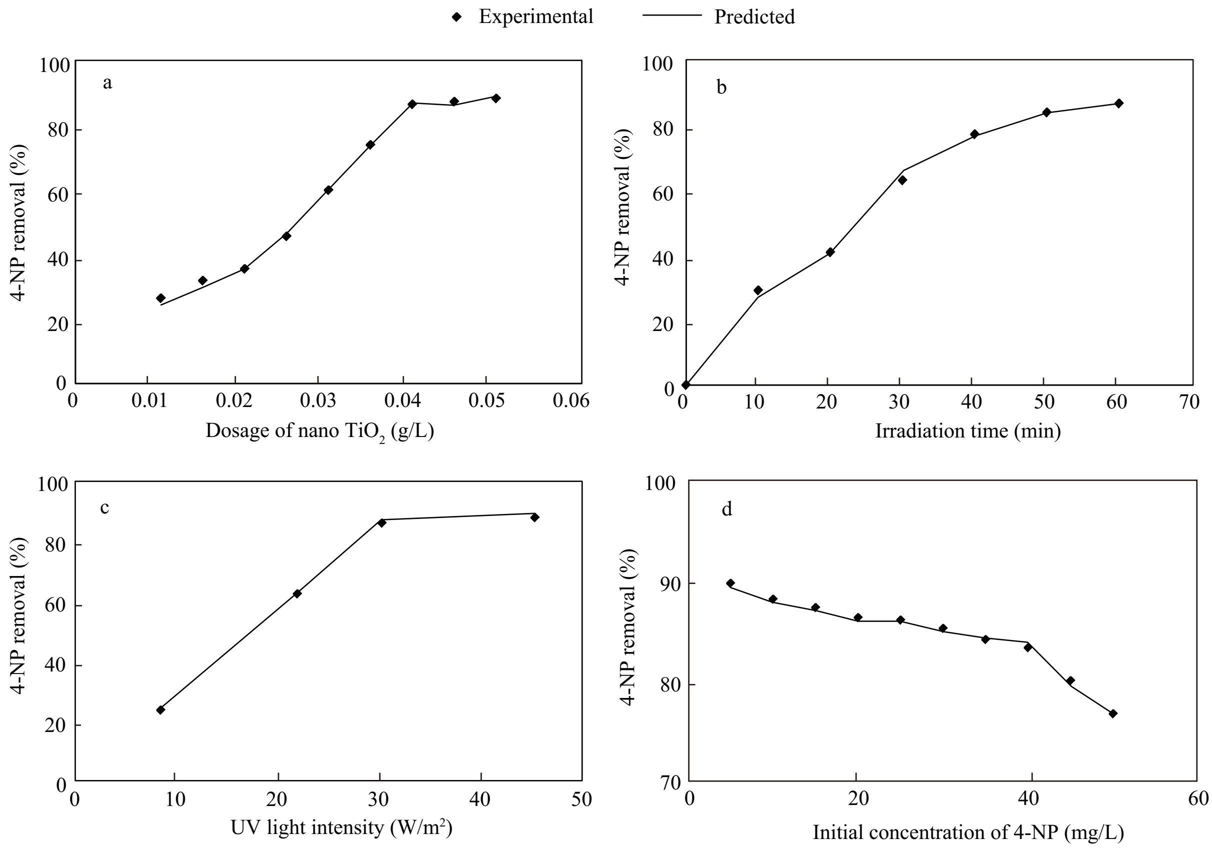

Fig. 7 Comparison between predicted ANN and experimental values of 4-NP removal with various factors. (a) nano TiO_2 dosage change; (b) effect of irradiation time; (c) effect of UV light intensity; (d) effect of 4-NP initial concentration. Other conditions: TiO_2 concentration 0.04 g/L, initial 4-NP concentration 20 mg/L, UV 30.3 W/m^2, 60 min.

increase of radiation intensity from 8.6 to 45.3 W/m^2, increases the removal from 24.13% to 84.26%. This increase is due to the enhanced production of hydroxyl radicals.

2.4.4 The 4-NP initial concentration

It is important from an application point of view to study the dependence of removal efficiency on the initial concentration of the 4-NP. Therefore, the effect of 4-NP concentration on the removal efficiency was investigated at different 4-NP initial concentrations. The experimental and ANN predicted values of 4-NP removal was plotted versus initial 4-NP concentration (Fig. 7d).

When the 4-NP concentration increases, the amount of 4-NP molecules adsorbed on the surface of the catalyst increases. This affects the photocatalytic activity of TiO_2 and reduce the photocatalytic efficiency. The increase in the 4-NP concentration also decreases the path of photons into the 4-NP solution. At high concentration, the 4-NP molecules may absorb a significant amount of light and this may also reduce the photocatalytic efficiency (Chakrabarti and Dutta, 2004).

3 Conclusions

TiO_2 prepared by sol-gel route was optimized using 4-NP during photocatalytic test. The results presented the anatase-type TiO_2 has higher photocatalytic activity than rutile type TiO_2 and in anatase phase the samples with small grain size have higher photocatalytic activity than the other's. A simulation based on the ANN model can estimate the behavior of the process under different conditions. One of the characteristics of modeling based on artificial neural networks is that it does not require the mathematical description of the phenomena involved in the process, and might be useful in simulating and up-scaling complex photochemical systems. The removal performance of 4-NP was successfully predicted by applying a three- layered neural network with 14 neurons in the hidden layer, and using back-propagation algorithm.

Acknowledgments

The authors would like to thank Prof. Ahmad Jafarian for his guidance related to the ANN modeling.

References

Aleboyeh A, Kasiri M B, Olya M E, Aleboyeh H, 2008. Prediction of azo dye decolorization by UV/H_2O_2 using artificial neural networks. *Dyes and Pigments*, 77(2): 288–294.

Ambrus Z, Mogyorósi K, Szalai ÁZolt'an A, K'aroly M, Ágnes S, Tünde Alapi T et al., 2008. Low temperature synthesis, characterization and substrate-dependent photocatalytic activity of nanocrystalline TiO_2 with tailor-made rutile to anatase ratio. *Applied Catalysis A: General*, 340(2): 153–161.

Bartram S F, Kaelble E F, 1967. Handbook of X-rays. McGraw-Hill, New York. 17: 1–17.

Behnajady M A, Modirshahla N, Daneshvar N, Rabbani M, 2007b. Photocatalytic degradation of an azo dye in a tubular continuous-flow photoreactor with immobilized TiO_2 on glass plates. *Journal of Chemical Engineering*, 127(1-3): 167–176.

Behnajady M A, Modirshahla N, Ghanbary F, 2007a. A kinetic model for the decolorization of C.I. Acid Yellow 23 by Fenton process. *Journal of Hazardous Materials*, 148(1-2): 98–102.

Bessekhouad Y, Robert D, Weber J V, Yassine B, Didier R, Jean V W, 2003. Synthesis of photocatalytic TiO_2 nanoparticles: optimization of the preparation conditions. *Journal of Photochemistry and Photobiology A: Chemistry*, 157(1): 47–53.

Calza P, Sakkas V A, Villioti A, Massolino C, Boti V, Pelizzetti E, Albanis T et al., 2008. Multivariate experimental design for the photocatalytic degradation of imipramine: Determination of the reaction pathway and identification of intermediate products. *Applied Catalysis B Environmental*, 84 (3-4): 379–388.

Castro A L, Nunes M R, Carvalho A P, Costa F M, Florêencio M H, 2008. Synthesis of anatase TiO_2 nanoparticles with high temperature, stability and photocatalytic activity. *Solid State Sciences*, 10(5): 602–606.

Chakrabarti S, Dutta B K, 2004. Photocatalytic degradation of model textile dyes in wastewater using ZnO as semiconductor catalyst. *Journal of Hazardous Materials*, 112(3): 269–278.

Chiou C H, Wu C Y, Juang R S, 2008. Influence of operating parameters on photocatalytic degradation of phenol in UV/TiO_2 process. *Journal of Chemical Engineering Journal*, 139(2): 322–329.

Daneshvar N, Khataee A R, Djafarzadeh N, 2006. The use of artificial neural networks (ANN) for modeling of decolorization of textile dye solution containing C. I. Basic Yellow 28 by electrocoagulation process. *Journal of Hazardous Materials B*, 137(3): 1788–1795.

Di Paola A, Cufalo G, Addamo M, Bellardita M, Campostrini R, Ischia M et al., 2008. Photocatalytic activity of nanocrystalline TiO_2 (brookite, rutile and brookite-based) powders prepared by thermohydrolysis of $TiCl_4$ in aqueous chloride solutions. *Colloids and Surfaces A: Physicochemical and Engineering Aspects*, 317(1-3): 366–376.

Giri Rabindra R, Ozmaki H, Takanami R, Tanighuchi S, 2008. A novel use of TiO_2 fiber for photocatalytic ozonation of 2,4-dichlorophenoxyacetic acid in aqueous solution. *Journal of Environmental Sciences*, 20(9): 1138–1145.

Göob S, Oliveros E, Bossmann S H, Braun A M, Guardani R, Nascimento C A O, 1999. Modeling the kinetics of a photochemical water treatment process by means of artificial neural networks. *Journal of Chemical Engineering*, 38(4-6): 373–382.

Gontarski C A, Rodrigues P R, Mori M, Prenem L F, 2000. Simulation of an industrial wastewater treatment plant using artificial neural networks. *Journal of Computers and Chemical Engineering*, 24(2-7): 1719–1723.

Habibi M H, Hassanzadeh A, Mahdavi S, 2005. The effect of operational parameters on the photocatalytic degradation of three textile azo dyes in aqueous TiO_2 suspensions. *Journal of Photochemistry and Photobiology A: Chemistry*, 172(1): 89–96.

Khataee A R, 2010. Photocatalytic removal of C.I. Basic Red 46 on immobilized TiO_2 nanoparticles: Artificial neural network modeling. *Environmental Technology*, 30(11): 1155–1168.

Khataee A R, Dehghan G, Zarei M, Ebadi E, Pourhassan M, 2011. Neural network modeling of biotreatment of triphenylmethane dye solution by a green macroalgae. *Journal of Chemical Engineering Research and Design*, 89(2): 172–178.

Khataee A R, Mirzajani O, 2010. UV/peroxydisulfate oxidation of C. I. Basic Blue 3: Modeling of key factors by artificial neural network. *Desalination*, 251(1-3): 64–69.

Modirshahla N, Behnajady M A, Ghanbary F, 2007. Decolorization and mineralization of C.I. Acid Yellow 23 by Fenton and photo-Fenton processes. *Dyes and Pigments*, 73(3): 305–310.

Muruganandham M, Swaminathan M, 2006. TiO_2–UV photocatalytic oxidation of Reactive Yellow 14: effect of operational parameters. *Journal of Hazardous Materials*, 135(1-3): 78–86.

Pareek V K, Brungs M P, Adesina A A, Sharma R, 2002. Artificial neural network modeling of a multiphase photodegradation system. *Journal of Photochemistry and Photobiology A: Chemistry*, 149(1-3): 139–146.

Rodrí′igerz J A, Ferná′andez-Garcí′ia M, 2007. Synthesis, Properties, and Applications of Oxide Nanomaterials. Wiley, New Jerky. 17: 135–160.

Slokar Y M, Zupan J, Le Marechal A M L, 1999. The use of artificial neural network (ANN) for modeling of the H_2O_2/UV decoloration process: part I. *Dyes and Pigments*, 42(2): 123–135.

Wen B M, Liu C Y, Liu Y, 2005. Optimization of the preparation methods: Synthesis of mesostructured TiO_2 with high photocatalytic activities. *Journal of Photochemistry and Photobiology A: Chemistry*, 173(1): 7–12.

Yan M C, Chen F, Zhang J L, Anpo M, 2005. Preparation of controllable crystalline titania and study on the photocatalytic properties. *Journal of Physical Chemistry B*, 109(18): 8673–8678.

Zhang J W, Fu D F, Xu Y D, Liu C Y, 2010. Optimization of parameters on photocatalytic degradation of chloramphenicol using TiO_2 as photocatalyist by response surface methodology. *Journal of Environmental Sciences*, 22(8): 1281–1289.

Zhang X, Wu F, Wu X W, Chen P Y, Deng D S, 2008. Photodegradation of acetaminophen in TiO_2 suspended solution. *Journal of Hazardous Materials*, 157(2-3): 300–307.

JOURNAL OF ENVIRONMENTAL SCIENCES

Journal of Environmental Sciences (Established in 1989)
Vol. 24 No. 4 2012

Supervised by	Chinese Academy of Sciences	**Published by**	Science Press, Beijing, China
Sponsored by	Research Center for Eco-Environmental Sciences, Chinese Academy of Sciences		Elsevier Limited, The Netherlands
Edited by	Editorial Office of Journal of Environmental Sciences (JES) P. O. Box 2871, Beijing 100085, China Tel: 86-10-62920553; http://www.jesc.ac.cn E-mail: jesc@263.net, jesc@rcees.ac.cn	**Distributed by** Domestic	Science Press, 16 Donghuangchenggen North Street, Beijing 100717, China Local Post Offices through China
		Foreign	Elsevier Limited http://www.elsevier.com/locate/jes
Editor-in-chief	Hongxiao Tang	**Printed by**	Beijing Beilin Printing House, 100083, China

CN 11-2629/X **Domestic postcode: 2-580** **Domestic price per issue RMB ¥ 110.00**

ISSN 1001-0742

9 771001 074123 04